iScience

CellPress
OPEN ACCESS

Article

Highly efficient hydrodesulfurization driven by an *in-situ* reconstruction of ammonium/amine intercalated MoS_2 catalysts

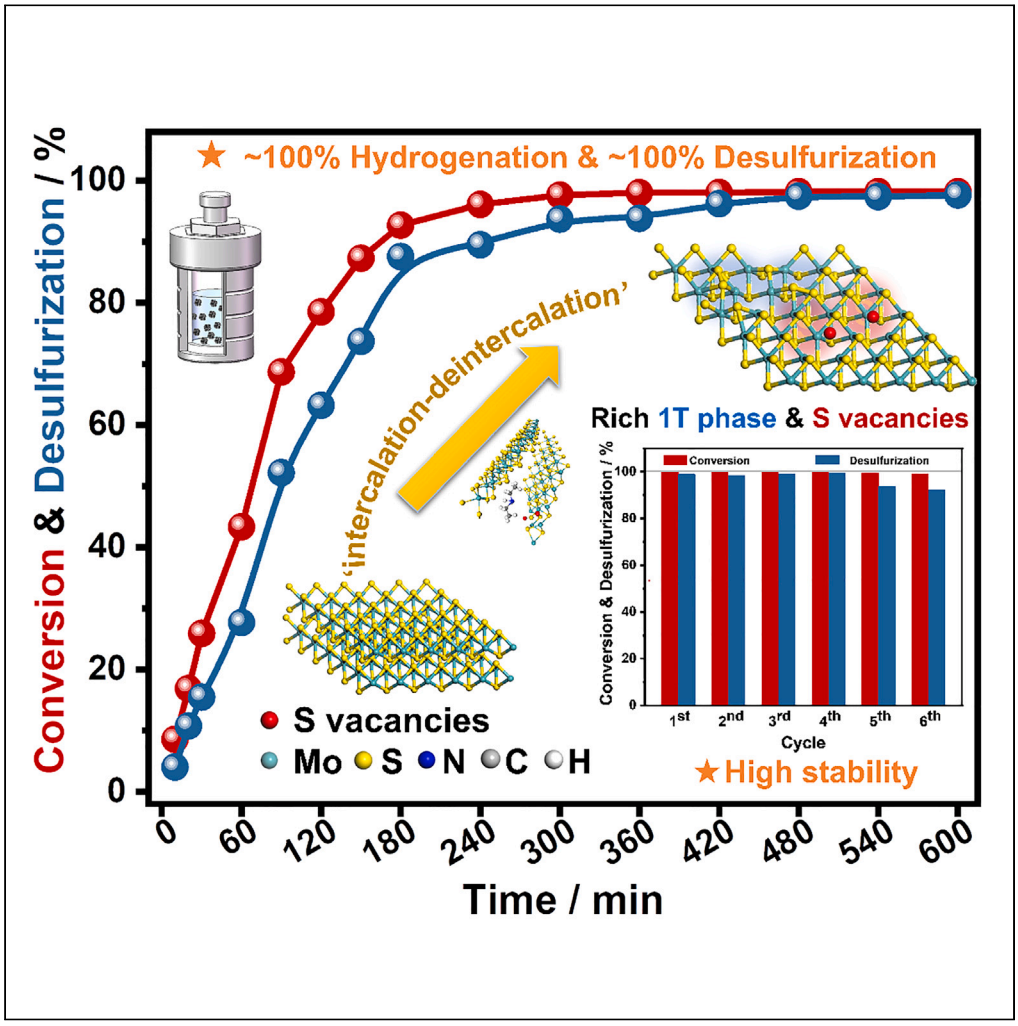

Tianlan Yan, Yingshuai Jia, Kaige Hou, ..., Qingsheng Gao, Yahong Zhang, Yi Tang

tqsgao@jnu.edu.cn (Q.G.)
yitang@fudan.edu.cn (Y.T.)

Highlights

Intercalating amine in MoS_2 produces high amount of 1T phase and S vacancies

Intercalation/deintercalation of MoS_2 generates abundant 1T phase and S vacancies

1T phase is conducive to hydrogenation, and S vacancy favors desulfurization

Yan et al., iScience *27*, 109824
June 21, 2024
https://doi.org/10.1016/j.isci.2024.109824

iScience

CellPress
OPEN ACCESS

Article

Highly efficient hydrodesulfurization driven by an *in-situ* reconstruction of ammonium/amine intercalated MoS_2 catalysts

Tianlan Yan,[1] Yingshuai Jia,[1] Kaige Hou,[1] Zhuxin Gui,[1] Wenbiao Zhang,[1,2] Ke Du,[1] Di Pan,[1] He Li,[1] Yanghao Shi,[2] Lu Qi,[3] Qingsheng Gao,[2,*] Yahong Zhang,[1] and Yi Tang[1,4,*]

SUMMARY

Hydrodesulfurization (HDS) is a commonly used route for producing clean fuels in modern refinery. Herein, ammonium/amine-intercalated MoS_2 catalysts with various content of 1T phase and S vacancies have been successfully synthesized. Along with the increment of 1T phase and S vacancies of MoS_2, the initial reaction rate of the HDS of dibenzothiophene (DBT) can be improved from 0.09 to 0.55 $\mu mol \cdot g_{cat}^{-1} \cdot s^{-1}$, accounting for a remarkable activity compared to the-state-of-the-art catalysts. In a combinatory study via the activity evaluation and catalysts characterization, we found that the intercalation species of MoS_2 played a key role in generating more 1T phase and S vacancies through the 'intercalation-deintercalation' processes, and the hydrogenation and desulfurization of HDS can be significantly promoted by 1T phase and S vacancies on MoS_2, respectively. This study provides a practically meaningful guidance for developing more advanced HDS catalysts by the intercalated MoS_2-derived materials with an in-depth understanding of structure-function relationships.

INTRODUCTION

With the increase of heavy oil component in crude oils and more strict regulations of environmental protection, there is an escalating worldwide demand for light cleaning oils.[1] However, the sulfur-containing impurities cause a series of fatal problems such as poisoning the catalysts and corroding equipment in the refinery process, while emitting harmful SO_2 from their combustion of the petroleum products and leading to serious environmental pollution as well as health problems.[2,3] The production of ultra-low sulfur fuel oil is essential to eradicate the unfavorable consequences. Nowadays, the developed ultra-deep desulfurization technologies are mainly composed of extraction desulfurization, adsorption desulfurization, oxidative desulfurization and hydrodesulfurization (HDS).[4,5] Among these approaches, HDS features the advantages of strong catalyst adaptability to feedstocks, long catalyst lifetime and process simplicity, which enable the efficient and wide application in oil refineries by removing refractory sulfur compounds, such as dibenzothiophene (DBT), 4-methyldibenzothiophene (4-MDBT), 4,6-dimethyldibenzothiophene (4,6-DMDBT) mostly found in heavy oils,[6,7] to produce clean oils with ultra-low sulfur content.

Designing high-efficient HDS catalysts is regarded as the straightforward yet desirable choice for further improvement of HDS technology.[8,9] Molybdenum disulfide (MoS_2) has gained great popularity in petroleum HDS due to its changeable edge structures and unique physicochemical properties.[10,11] Generally, MoS_2 predominantly exists in two crystal phases, i.e., 1T and 2H.[12] 2H MoS_2 is a thermodynamically stable phase containing A-b-A sandwich-like layers with edge-sharing [MoS_6] trigonal prisms, while the metastable 1T MoS_2 has been reported to have A-b-C layers with edge-sharing [MoS_6] octahedra.[13] According to crystal field theory, different atomic arrangements of MoS_6 unit result in distinct splitting of Mo 4d orbitals, leading to a different progressive filling of nonbonding d bands.[14] Thus, the electronic properties of 1T-MoS_2 are dramatically different from 2H-MoS_2.[15] Considerable theoretical and experimental researches have been devoted to investigating the active sites over MoS_2.[16–18] For HDS reaction, traditional view advocates that the catalytic ability of hydrogenation and cleavage of C-S bonds are indispensable. H_2 dissociation is a key step in hydrogenation via homolytic or heterolytic pathway.[19,20] Recent research showed that H_2 can be easily dissociated on 1T-phase MoS_2 compared with 2H-phase MoS_2.[21] Additionally, it is generally accepted that the S vacancies located at the edges of Mo or S can serve as active sites in the HDS process. This is owing to the fact that S vacancies serve as chemisorption sites, lowering the activation energy barrier for reactions involving sulfur compounds and promoting the cleavage of C-S

[1]Department of Chemistry, Shanghai Key Laboratory of Molecular Catalysis and Innovative Materials, and, Laboratory of Advanced Materials, Fudan University, Shanghai 200433, P.R. China
[2]College of Chemistry and Materials Science, and, Guangdong Provincial Key Laboratory of Functional Supramolecular Coordination Materials and Applications, Jinan University, Guangzhou 510632, P.R. China
[3]School of Petrochemical Engineering, and, Jiangsu Key Laboratory of Advanced Catalytic Materials and Technology, Changzhou University, Changzhou, Jiangsu 213164, P.R. China
[4]Lead contact
*Correspondence: tqsgao@jnu.edu.cn (Q.G.), yitang@fudan.edu.cn (Y.T.)
https://doi.org/10.1016/j.isci.2024.109824

bonds in sulfur-containing compounds.[22] Based on the previous studies, as an ideal HDS catalyst, MoS_2 should possess more 1T phase and abundant S vacancies.

Although numerous strategies, including morphological regulation (stacked layers and size), defect engineering and metal doping, were developed to improve the HDS performance of MoS_2, the symbiosis of 1T-2H MoS_2 were rarely reported to the best of our knowledge.[23–25] The original discussion of 1T-2H MoS_2 in HDS system could date back to the report of Cao and co-workers in 2020, in which DBT conversion of ~80% was obtained over 63.5% 1T phase MoS_2-water-ethanol-gly catalyst prepared by solvothermal method under the environment of water, ethanol, and glycerin.[26] Further studies were also carried out in 2022 using oxalic acid in place of glycerol to further increase the fraction of 1T phase in MoS_2. By regulating oxalic acid in the mixture of ethanol and water, the synthesized MoS_2-water-ethanol-OA with 79.7% of 1T phase showed the highest DBT conversion of 89.3% and an HYD selectivity of 88% after 10 h.[27] Later on, Wei et al. reported that, the MS-50 (~48% 1T phase) prepared with 50% ethanol showed the highest HDS conversion of DBT (84.2%), and the selectivity of BP was as high as 70.2%.[28] These studies found that the fresh 1T-2H MoS_2 catalysts possess an expanded interlayer spacing, while the catalytic performance of HDS was greatly enhanced by increasing the proportion of 1T phase in MoS_2. Significantly, the selectivity of products on MS-50 was quite different compared with the former two catalysts. However, in-depth explanations still required to clarify the unique catalytic behaviors of coexisting 1T-2H MoS_2 for HDS. On the other hand, several researchers have observed the reconstruction under reaction conditions, such as the smaller interlayer space along the c-axis and the reduced 1T phase content of MoS_2 after HDS.[27,28] However, its structure-activity relationship was primarily established on the characterizations and catalytic performance of the fresh catalysts (i.e., before reconstruction), which may not be persuasive. Meanwhile, the impacts of intercalation agents and the induced *in-situ* reconstruction under HDS conditions have not been mentioned on the structure and corresponding HDS performance of expanded-MoS_2 catalysts in the previous reports. Therefore, a deep insight is urgently essential to reveal the mechanism and real active sites of expanded 1T-2H MoS_2 catalysts in HDS.

Here, the ammonium/amine-intercalated 1T-2H MoS_2 nanosheets with varied interlayer spacings were successfully employed for the first time in the HDS process. The intercalated MoS_2 samples with inorganic ammonium content from low to high were denoted as MoS_2-LA and MoS_2-HA, respectively, while the intercalation of organic amine produced MoS_2-OA. During the HDS process of DBT, the specific reaction rate improved from 0.09 to 0.21 $\mu mol \cdot g_{cat}^{-1} \cdot s^{-1}$ with the increase of intercalated ammonium content. To achieve a superior performance of HDS, MoS_2-OA with the intercalated organic amine can surprisingly obtain a high reaction rate of 0.55 $\mu mol \cdot g_{cat}^{-1} \cdot s^{-1}$. Meanwhile, high DBT conversion of 100% and a high ultra-deep sulfur removal of 98.9% can be well accomplished over MoS_2-OA, which also exhibited excellent stability even after six consecutive catalytic runs. The comprehensive characterization showed that the excellent activities were highly connected with the abundant content of 1T phase and S vacancies generated by *in-situ* construction of intercalated MoS_2. The 1T phase was beneficial for boosting the hydrogenation while the S vacancies would facilitate the desulfurization. Compared with inorganic ammonium, the intercalation of organic amine in MoS_2 would generate higher amounts of 1T phase and S vacancies, while *in situ* S vacancies during HDS can further enhanced by the reconstruction induced by the deintercalation of interlayer species. Our investigation offers new insights into the intercalated MoS_2 to realize highly efficient HDS via regulating the 'intercalation-deintercalation' processes.

RESULTS AND DISCUSSION

Synthesis and characterization of ammonium/amine-intercalated MoS_2 catalysts

The ammonium/amine-intercalated MoS_2 catalysts were prepared via a hydrothermal method referring to our previous reports,[29,30] as depicted in Scheme 1 (see Experimental procedures for more details). The 1T-enriched MoS_2 with expanded and tunable interlayer spacing would be produced by introducing ammonium (NH_4^+) or dimethylamine cations (DMA^+), which would serve as the intercalants to inhibit the order growth of MoS_2 nanosheets, forming a disordered basal plane with abundant dislocations and distortions.

Figure 1A depicts the XRD patterns of the samples and the standard pattern of MoS_2 (JCPDS 37–1492). The MoS_2-LA showed the typical peaks of MoS_2. However, a significant shift in the peak corresponding to (002) plane was observed from the 2θ value of 14.4° to 9.4° for MoS_2-HA and to 9.0° for MoS_2-OA due to the NH_4^+ and DMA^+ intercalation between the layers of MoS_2.[29,30] It's indicated that their interlayer spacings have been substantially expanded from 6.2 Å to about 9.4 Å and 9.8 Å, respectively. A peak appearing around 17.8° corresponds to the (004) diffraction provides additional support for the expanded interlayer spacing.[31] Two broadened peaks at centered 32° and 57° can be well indexed to (100) and (110) planes, suggesting the same atomic arrangement along the basal planes.[32] The results indicate that MoS_2 with different lattice expansion were successfully obtained in the regulation of hydrothermal time or guest intercalants.

The morphology and intercalated structure of aforementioned MoS_2 catalysts can be further characterized by scanning electron microscope (SEM), transmission electron microscope (TEM) and high-resolution TEM (HRTEM). According to the SEM images (Figure 1B), the MoS_2 samples exhibit uniformly spherical nanoflowers (~250 nm) with wrinkled surface and are composed of flake-like sheets. Typical fringes of MoS_2 were observed in the TEM micrographs of all MoS_2 catalysts (Figure 1C). Most of the MoS_2 nanoflower particles consist of about ten layers with a length range of 200–250 nm. The hydrothermal time and the introduction of N,N-dimethylformamide (DMF) in precursor solutions have no obvious effect on the morphology of the MoS_2 nanosheets. The HRTEM images of MoS_2-LA, MoS_2-HA and MoS_2-OA showed lamellar pattern with an interlayer spacing of 0.62, 0.94 and 0.98 nm, respectively, further confirming the existence of the inserted species in MoS_2-HA and MoS_2-OA. Additionally, the HRTEM image of MoS_2-OA revealed the defect-rich feature and relatively disordered atomic arrangement along the basal planes, as evident by the presence of abundant dislocations and distortions (indicated by the red circles in Figure 1C). The selected area electron diffraction (SAED) showed a pattern of concentric rings (inset in Figure 1C), revealing the polycrystalline nature of MoS_2 catalysts.[12]

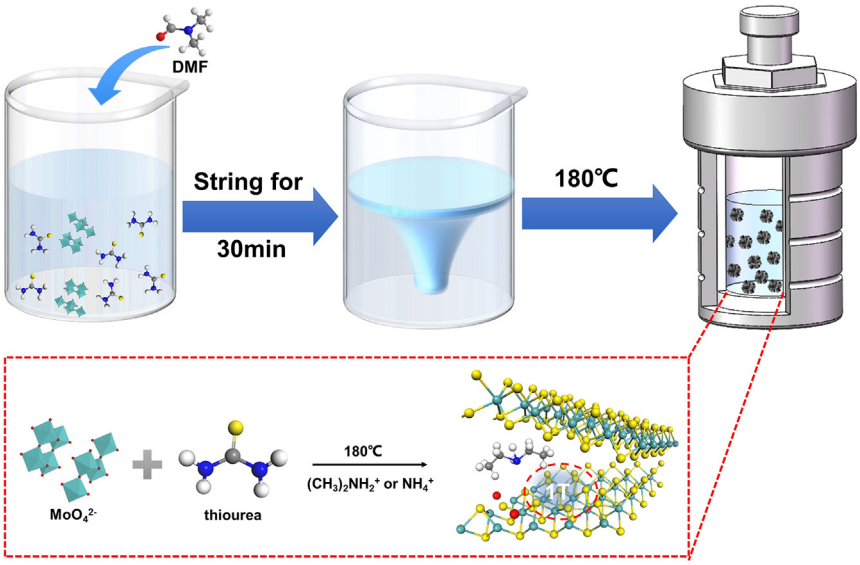

Scheme 1. The preparation process of ammonium/amine-intercalated MoS_2 catalysts

The phase identification of the fresh MoS_2 catalysts was studied using X-ray photoelectron spectroscopy (XPS).[33] Figure 2A presents the Mo 3d XPS spectra of three MoS_2 catalysts, from which the content of 1T phase is semi-quantitatively determined. The Mo 3d peaks are deconvoluted to two chemical states, the peaks at 228.6 ($3d_{5/2}$) and 231.7 eV ($3d_{3/2}$) correspond to the 1T phase and the ones at 229.1 ($3d_{5/2}$) and 232.4 eV ($3d_{3/2}$) are for the 2H phase.[34] Accordingly, the contents of the 1T phase were estimated (Table 1). The MoS_2-LA obtained with longer hydrothermal time has a ~40.4% 1T-MoS_2 phase, and its 1T/2H ratio is 0.68. MoS_2-HA synthesized in short time exhibited predominantly 1T-MoS_2 phase. The MoS_2-OA sample in the hydrothermal system containing DMF possesses the highest content of the 1T phase, that is, ~65.0% with a 1T/2H ratio of 1.85. A similar trend is obtained from the deconvolution of the S 2p XPS spectra (Figure 2A). Moreover, a remarkable N 1s peak is also observed at 401.9 eV, which can be attributed to the existence of NH_4^+ and DMA^+. This demonstrates the successful intercalation of guest species into the MoS_2-HA and MoS_2-OA, consistent with the XRD and HRTEM results.[35]

To verify the formation of the 1T phase of MoS_2, the Raman spectrum of the fresh catalysts was also collected. The crystal structural variations in 1T-MoS_2 and 2H-MoS_2 can be easily distinguished from their Raman spectra, as shown in Figure 2B.[36] The Raman shifts located at 147 (J_1), 195, 235 (J_2), 283(E^1_g) and 335 (J_3) cm^{-1} correspond to the characteristic phonon vibration patterns of 1T MoS_2.[21,37,38] The weak peaks at 376.1 cm^{-1} and 403.4 cm^{-1} can be attributed instead to the in-plane (E^1_{2g}) and out-of-plane (A_{1g}) vibration mode of 2H-phase MoS_2.[39] It can be concluded that all the fresh MoS_2 catalysts possess a hybrid phase of 1T and 2H.

Electron paramagnetic resonances (EPR) can be considered as a powerful tool to estimate the concentration of S vacancies in all catalysts.[40] They exhibit a significant paramagnetic signal at g = 2.004 in Figure 2C, and the peak intensity is proportional to the concentration of Mo-S dangling bonds originating from the presence of single S vacancies in the MoS_2 nanosheets.[41] The peak intensities increased in the order MoS_2-LA < MoS_2-HA < MoS_2-OA, indicating that the coordinatively unsaturated S^{2-} content in MoS_2 increased as the interlayer spacing increases.

The H_2-temperature programmed reduction (H_2-TPR) curves of the fresh MoS_2 catalysts are shown in Figure 2D. It was found that all the catalysts exhibited two reduction peaks, including a peak at ~220°C, originating from the sulfur atoms that are weakly bonded to the MoS_2 particle on the catalyst surface, especially originating from the reduction of S-S dimmers or bridging S atoms at the edges of the MoS_2 nanoclusters, and a broad peak at ~350°C, corresponded to the partial reduction of the small MoS_2 crystals.[42] In the range of 120°C and 320°C, the TPR peak area of MoS_2-LA was minimal among those of all the MoS_2 samples. MoS_2-HA, possessing 63.2% 1T phase and few vacancies, already exhibited a larger low-temperature peak, which moved toward lower temperature. The largest peak area for the MoS_2-OA demonstrates the abundant active sites as compared with MoS_2-LA and MoS_2-OA. Therefore, it is reasonable to expect that the MoS_2-OA exhibits superior performance in the HDS reaction.

Thermogravimetry (TG) measurements on MoS_2 catalysts were also performed to confirm the presence of the guest species. As depicted in Figure 2E, the obtained MoS_2 catalysts underwent gradual decomposition on heating as evidenced by their TG curves. TG curves of the fresh MoS_2 samples suggested the presence of intercalated species that deintercalated at different temperatures. In the case of MoS_2-LA and MoS_2-OA, we observe an obvious single-step mass loss center around ~260 and ~285°C, respectively, while in MoS_2-HA there were two distinct mass loss steps centered around ~80 and ~240°C. According to the TG results, the selected reaction temperature (320°C) is high enough to ensure that almost all inorganic/organic components can be removed from the catalyst surface.

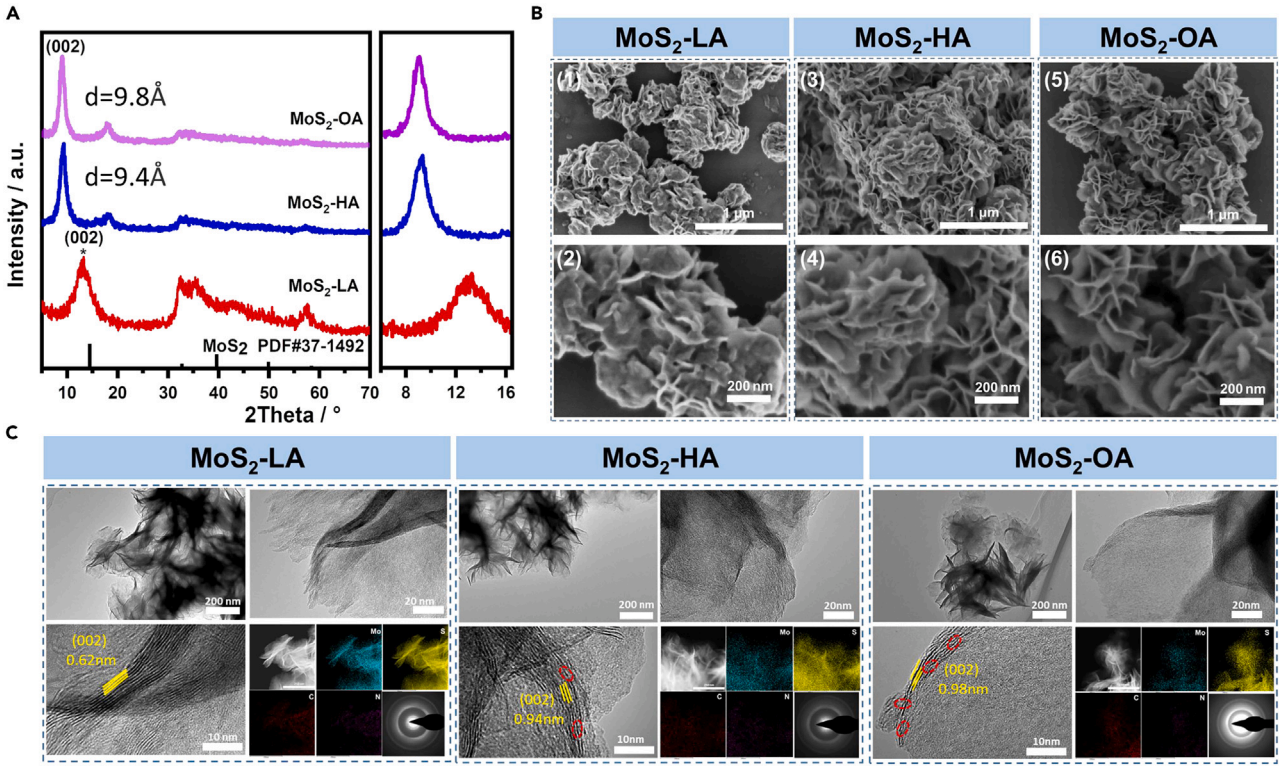

Figure 1. Structural and morphology characterization of MoS_2 catalysts

(A) XRD pattern of MoS_2 catalysts.

(B) SEM image of MoS_2 catalysts.

(C) TEM images of MoS_2 catalysts.

Catalytic activity assessment

HDS of DBT on MoS_2 catalysts

The catalytic performance of all fresh MoS_2 catalysts was evaluated for the HDS of DBT (Figure 3A). All the catalysts yield the same products such as BP, THDBT, HHDBT, CHB, BCH, CPMB, and CPMC, among which CHB is the main product of all catalysts. Under the same reaction conditions, the activities of these catalysts increased in the order MoS_2-LA < MoS_2-HA < MoS_2-OA. Obviously, MoS_2-OA can achieve 100% conversion of DBT and the high ultra-deep sulfur removal of 98.9% even the catalyst amount was as low as 50 mg. It seems that the insertion of NH_4^+ or DMA^+ ions can induce an increase in the interlayer spacing of MoS_2, resulting in a significant enhancement in activity for the HDS of DBT compared with MoS_2-LA. However, XRD patterns of the used catalysts revealed a shift in the diffraction peak corresponding to the MoS_2 (002) plane toward to a higher angel of approximately 14.4° (Figure 3B), implying that the interlayer species might disappear after HDS reaction at 320°C. The TEM also demonstrates this result while the morphology, size and laminate stacking number of the MoS_2 particles were almost no changes in the used catalysts (Figure S1). We firstly selected the most active MoS_2-OA to understand the role of inserted species in enhancing HDS performance, and found that the performance was essentially stable in the second cycle (Figure S2). It's suggested that the catalytic activity may be not affected by the expanded layer structure and interlayer species. Meanwhile, XPS, Raman and EPR experiments were conducted further to explore the phase and S vacancies content of used MoS_2 catalysts. The results revealed that there was an increase in S vacancies, while the 1T phase content was basically maintained compared to fresh MoS_2 catalysts(Figures 3C–3E), probably due to the role of S vacancies in the stabilization of 1T.[43] In addition to the generation of S vacancies and 1T phases due to NH_4^+ and DMA^+ insertion in the synthetic process, three samples also exhibited an enhancement in S vacancies after the HDS reaction, indicating that the deintercalation of ammonium/amine is favorable for the further generation of S vacancies. It is concluded that MoS_2-LA undergoes slight but inevitable reconstruction during the HDS reaction.[44] Compared with the used MoS_2-LA, the used MoS_2-HA and used MoS_2-OA possess more 1T phase and S vacancies (1.4–1.6 times vs. 2.4–3.8 times). This suggested that whether ammonium or amine intercalation into MoS_2 can further induce the *in-situ* reconstruction, the latter is more effective in promoting the reconstruction. Thus, MoS_2-OA possessed the superior HDS performance thanks to the highest content of 1T phase and S vacancies that were *in situ* derived from the 'intercalation-deintercalation' of interlayer species.

Meanwhile, the similar initial reaction rate on the fresh and used (~0.56 $\mu mol \cdot g_{cat}^{-1} \cdot s^{-1}$) MoS_2-OA implies the rapid reconstruction of the catalyst during the initial reaction (Figure S3). Furthermore, the shrinkage of the MoS_2-OA interlayer spacing was observed after HDS in 10 min

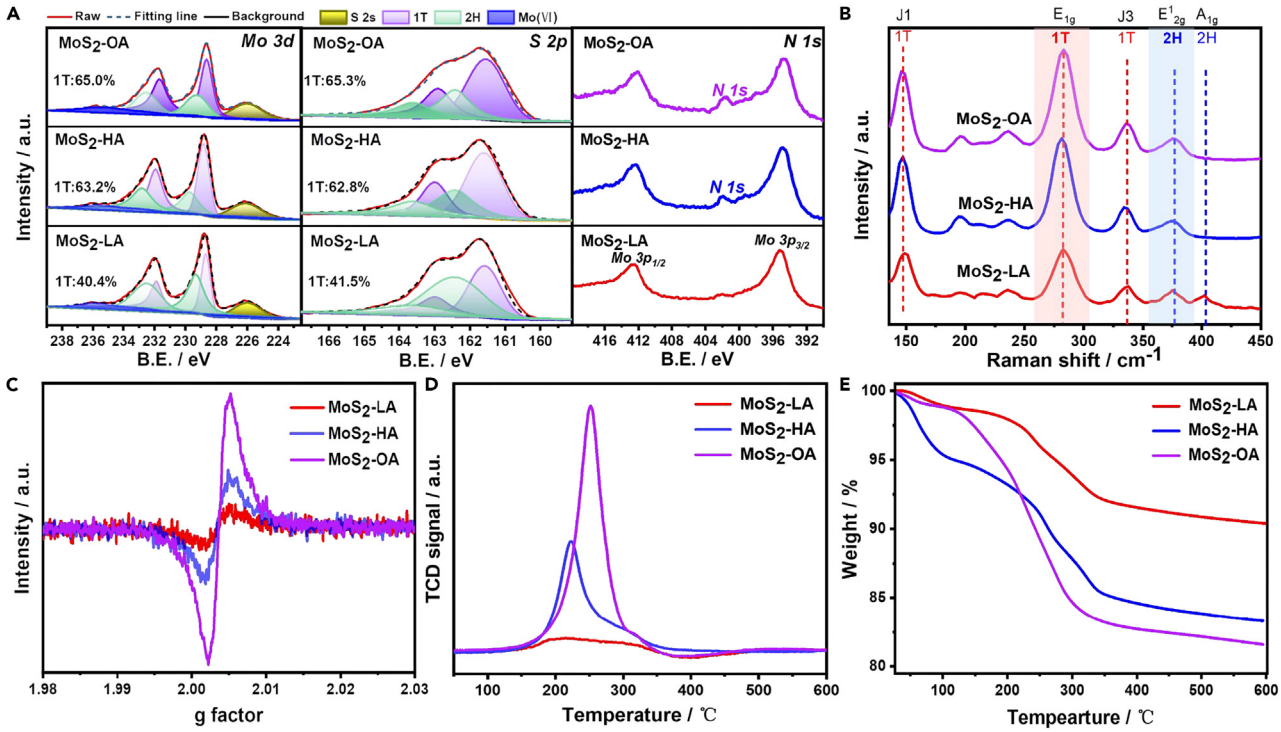

Figure 2. XPS, Raman, EPR, H_2-TPR and TG spectra of MoS_2 catalysts

(A) XPS of Mo 3d, S 2p and N1s for MoS_2 catalysts.

(B) Raman spectra of MoS_2 catalysts.

(C) EPR spectra of MoS_2 catalysts.

(D) H_2-TPR results of MoS_2 catalysts.

(E) TG spectra of MoS_2 catalysts.

(reduced to 6.3 Å, as evidenced by XRD and HRTEM in Figures S4 and S5), suggesting that the reconstruction has been completed in the very early stage of HDS. Therefore, the catalytic performance of fresh MoS_2 can reflect the behavior of catalysis after *in-situ* reconstruction of HDS, and the characterization of used catalysts may represent the state of those under the reaction conditions.

Hydrogenation of BP and CHB on used MoS_2 catalysts

The HDS process involves hydrogenation and desulfurization.[45] We first investigated the hydrogenation performance of used MoS_2 catalysts by using model compounds of BP and CHB (typical HDS products of DBT) under the same reaction conditions (Figure 3F). Using used MoS_2-OA with the highest proportion of 1T-phase as a catalyst, the conversion of BP and CHB reached 39.0% and 4.9%, respectively. Results show that both BP and CHB can be hydrogenated, and BP is much easier for hydrogenation than that of CHB while CHB is scarcely further hydrogenated. Considering the actual conditions of HDS, we further investigated the BP hydrogenation on MoS_2-OA in the presence of benzothiophene. The existence of H_2S has no influence on the hydrogenation products of BP. No other products, including isomerized and cracking products, were detected, indicating that the used MoS_2 cannot catalyze the skeletal rearrangement of cycloalkanes and the cleavage of C-C bonds.[46]

The BP conversion on used MoS_2-OA was found to be 3.9 times higher than that of used MoS_2-LA and 1.8 times higher than that of used MoS_2-HA (Figure 3F), that is, the hydrogenation activity of the MoS_2 catalysts ranked as follows: used MoS_2-OA > used MoS_2-HA > used MoS_2-LA. These results suggest a strong relationship between the hydrogenation capability and the 1T phase content, because the 1T phase in MoS_2 is essential for the dissociation and activation of H_2, which can be corroborated by XPS and H_2-TPR results.[21]

Table 1. 1T-2H Percentages and atomic ratios of S/Mo for different samples derived from the XPS spectra

Samples	1T/%	2H/%	S/Mo
MoS_2-LA	40.4	59.6	1.86
MoS_2-HA	63.2	36.8	1.77
MoS_2-OA	65.0	35.0	1.74

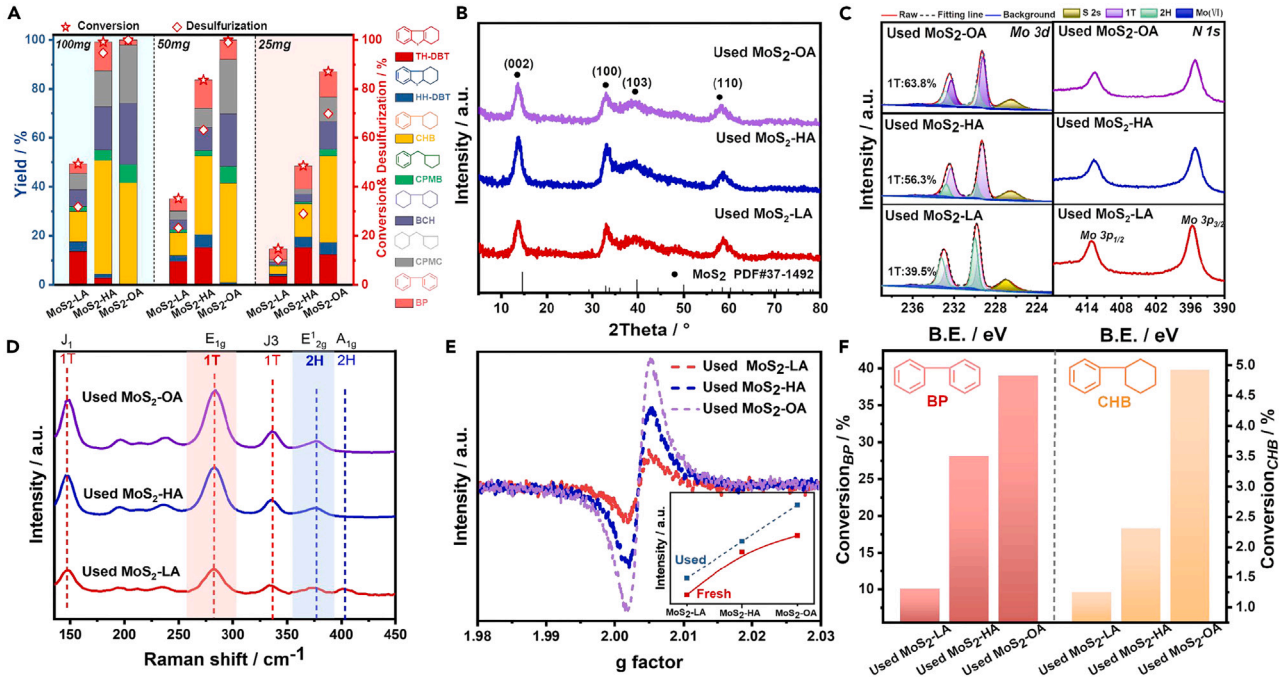

Figure 3. Catalytic performance and structural characterization of MoS_2 catalysts

(A) Catalytic HDS performance of MoS_2 catalysts after 8 h.

(B–E) (B)XRD, (C)XPS, (D) Raman and (E) EPR of used MoS_2 catalysts.

(F) The hydrogenation performance of used MoS_2 catalysts after 8 h.

HDS kinetics and possible reaction network

For the further development of high-performance HDS catalysts, an in-depth understanding of the HDS reaction mechanisms and kinetics of sulfur-containing molecules over these MoS_2 catalysts are indispensable. A precise comparison among activities of all fresh catalysts was made by measuring the reaction rate and product yields in the HDS as a function of reaction time. Such catalysts were tested under the identical reaction conditions. As depicted in Figures 4A–4C, the primary product over all catalysts is CHB. As reaction time was prolonged, the yield of CHB, BCH, CPMB and CPMC gradually increased and then remained at a certain level. Whereas the yield of THDBT and HHDBT increased rapidly first, and then depleted eventually with the subsequent consumption. And the content of BP also increased first and then diminished due to the hydrogenation.

It's commonly accepted that THDBT, HHDBT, CHB, CPMB, BCH and CPMC are the main products for the hydrogenation (HYD) pathway, while BP is the product of the direct hydrodesulfurization (DDS) pathway.[47,48] Considering that BP and CHB may be further hydrogenated, the ascription of reaction pathways on the HDS of DBT requires some caution, especially for MoS_2-HA and MoS_2-OA (Figures 4A and 4B). Taking MoS_2-OA for instance, the complicated HDS process was divided into three consecutive stages: (I) Initial → (II) Middle → (III) Later stages. In the initial stage, the secondary reactions scarcely occurred at a lower conversion (<25%). The middle stage primarily involves the transformation of partial hydrogenation sulfur-containing intermediates such as THDBT and HHDBT. The later stage mainly involves BP conversion. The process on MoS_2-HA is similar to the aforementioned one. However, only the first two stages are observed on MoS_2-LA, which is attributed to its inadequate performance.

First, during the stage (I) with low conversion, in order to distinguish the difference among three catalysts on HDS, the reaction rate and the selectivity of product by reaction routes on MoS_2 catalysts were calculated and summarized in Table 2. The r_{HDS} over the MoS_2-OA catalyst reaches 0.55 $\mu mol \cdot g_{cat}^{-1} \cdot s^{-1}$, which is approximately 6.3 times greater than that over MoS_2-LA catalyst (0.09 $\mu mol \cdot g_{cat}^{-1} \cdot s^{-1}$) and 2.6 times greater than that over the MoS_2-HA catalyst (0.21 $\mu mol \cdot g_{cat}^{-1} \cdot s^{-1}$). During the initial stage, the hydrogenation of BP to CHB is negligible in the presence of sulfur-containing compounds, which means that the selectivity of BP can be used as a criterion of the DDS pathway and the selectivity of others products (CHB, etc.) representing the HYD pathway.[47,48] Both k_{DDS} and k_{HYD} over MoS_2-OA are higher than those of MoS_2-HA due to its higher amount of 1T and S vacancies, and the k_{DDS} and k_{HYD} of MoS_2-LA are lowest in these three samples due to its least active sites.[26–28] For MoS_2-OA, the $S_{HYD/DDS}$ is up to 3.26, much higher than that of MoS_2-HA (1.86), indicating the enhancement of HYD is more significant. On the contrary, MoS_2-LA possesses a slightly lower $S_{HYD/DDS}$ value (1.76), meaning the decrease of HYD is relatively faster. Nevertheless, the $S_{HYD/DDS}$ were much higher than 1 indicating that the HYD route is a more favorable route over all catalysts.

In the middle stage (II) of HDS, in comparison with MoS_2-HA, it can be observed that the THDBT has been accumulated at a more rapid rate on MoS_2-OA. The higher reaction rate and HYD selectivity of MoS_2-OA with the highest 1T phase content are responsible for this. When the

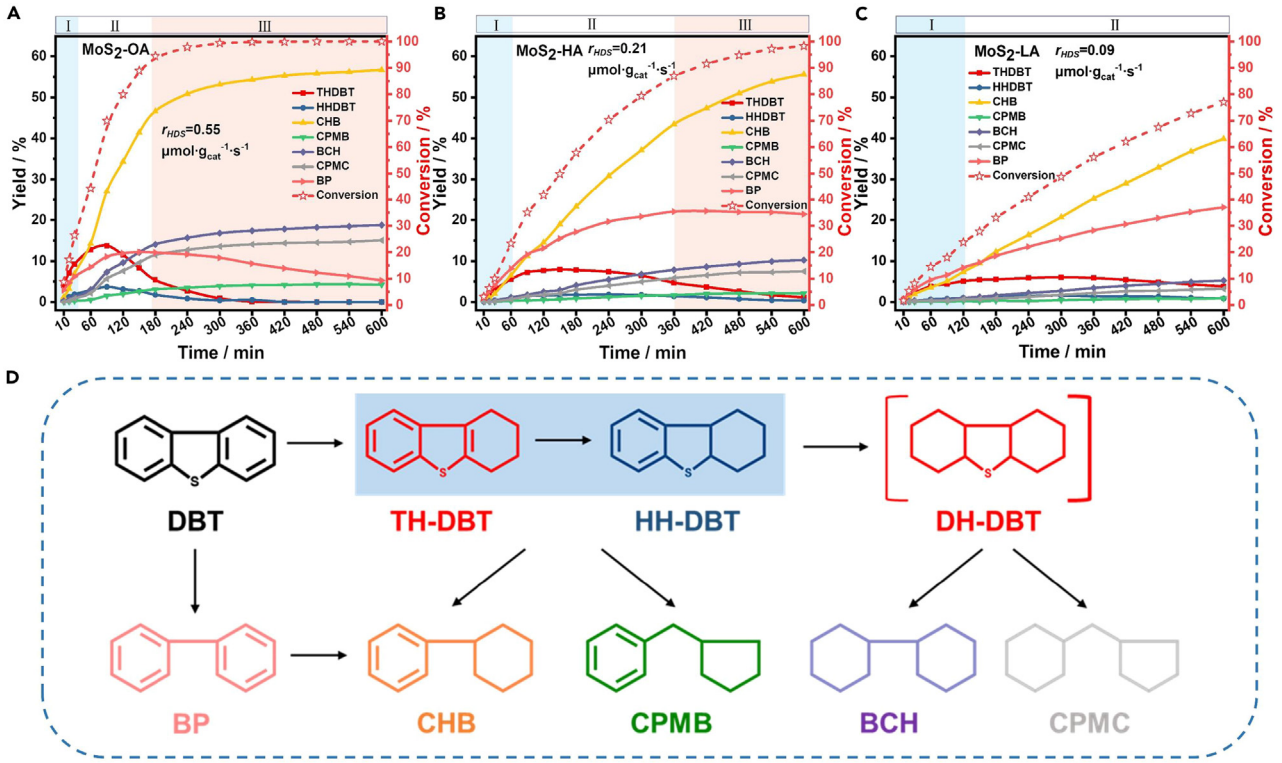

Figure 4. Catalytic HDS performance of MoS_2 catalysts and proposed reaction network

(A–C) Conversion and product yields as function of reaction time for the HDS of DBT over (A) MoS_2-OA, (B) MoS_2-HA and (C) MoS_2-LA catalysts, respectively. (D) Proposed reaction network for the DBT HDS.

reactants have been largely consumed, the accumulated THDBT can be consumed faster and vanished quickly within 6 h, which is apparently shorter than that of MoS_2-HA (>10 h). The higher S vacancies in MoS_2-OA could be the reason for this, according to the EPR results in Figure 3E. Although MoS_2-OA possesses the highest S vacancies, the high hydrogenation ability leads to the overproduction of THDBT beyond its desulfurization capabilities resulting from the S vacancies. Additionally, THDBT will compete with the DBT reactant and other sulfur-containing products for active sites, such as HHDBT and DHDBT with faster desulfurization rate due to their lower C-S bond cleavage barriers.[49,50] In contrast, MoS_2-LA is the slowest catalyst in terms of THDBT formation because of its lowest 1T phase content, and consumed slowly due to having the least S vacancies. In summary, it can be concluded that 1T-phase plays an essential role in achieving highly efficient HDS, while it should also be noted that the S vacancies are also indispensable.

When the HDS reaction proceeds to the (III) latest stage, the BP yield declined rapidly on the MoS_2-HA and MoS_2-OA due to its further hydrogenation.[51,52] The MoS_2-OA exhibited a lower accumulation of BP and faster decrease rate originating from its high hydrogenation ability, aligned with the BP hydrogenation performance as above-mentioned in Figure 3F.

Based on the above study, we propose the reaction networks for the HDS of DBT over the MoS_2 catalysts, as depicted in Figure 4D. The HDS of DBT includes two reaction routes for sulfur removal.[47,48] One is the HYD pathway, which involves hydrogenation of one or both aromatic rings prior to C-S bond hydrogenolysis, primarily the hydrogenation into partially hydrogenated sulfur-containing intermediates, and subsequently desulfurization toward CHB, BCH and isomerized products CPMB and CPMC. The other is a DDS pathway, which involves

Table 2. HDS of DBT analysis results over MoS_2- OA, MoS_2-HA, and MoS_2- LA catalysts[a]

Samples	r_{HDS}[a] ($\mu mol \cdot g_{cat}^{-1} \cdot s^{-1}$)	r_{HYD}[a] ($\mu mol \cdot g_{cat}^{-1} \cdot s^{-1}$)	r_{DDS}[a] ($\mu mol \cdot g_{cat}^{-1} \cdot s^{-1}$)	$S_{HYD/DDS}$[b]	S_{ISO}[c] (%)
MoS_2-OA	0.55	0.42	0.13	3.26	4.19
MoS_2-HA	0.21	0.14	0.07	1.86	4.03
MoS_2-LA	0.09	0.06	0.03	1.76	2.79

[a]Reaction rate was calculated at low conversion.
[b]DDS = BP, HYD = THDBT + HHDBT + CHB + CPMB+ BCH + CPMC.
[c]ISO = CPMB + CPMC.

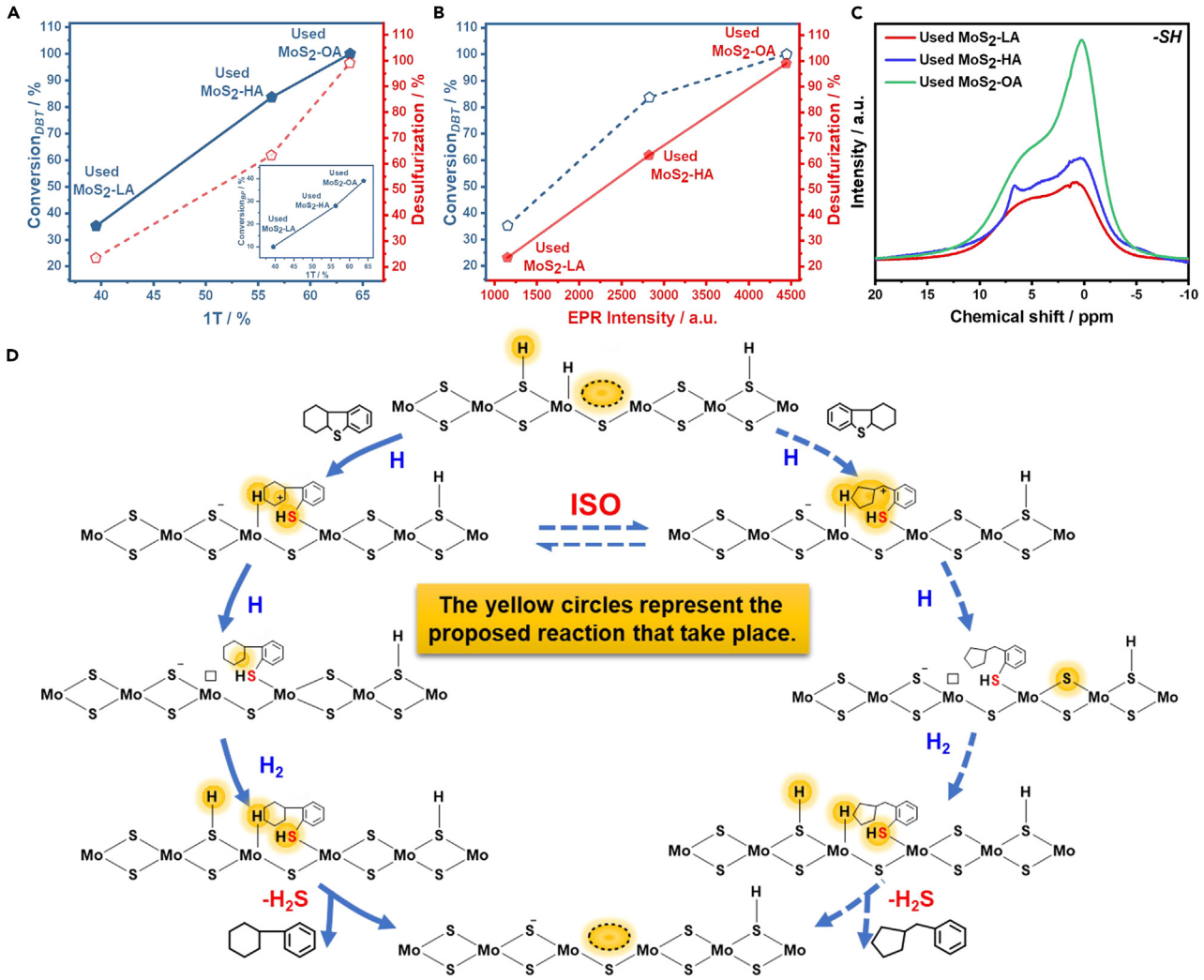

Figure 5. Investigation of the HDS mechanism on MoS_2 catalysts

(A and B) Catalytic performance between functional sites.

(C) ^{1}H NMR of used MoS_2 catalysts.

(D) Proposed mechanism for THDBT isomerization on MoS_2.

direct hydrogenolysis of the C-S bond of thiophene ring without hydrogenation of the aromatic rings, and ultimately leads to BP as the hydrocarbon product.[52] Both HYD and DDS pathways play an important role in the DBT HDS, while the HYD pathway is considered to be dominant for the DBT molecule to realize the final sulfur removal for all fresh catalysts. In comparison, the enhancement of HYD pathway on MoS_2-OA was stronger than that on the DDS pathway.

The aforementioned study found that BP can be hydrogenated to CHB, and BP cannot be used as a criterion for DDS pathway as decreasing concentrations of BP were observed under the conditions of higher conversion. And BP can represent the DDS pathway at low conversion since BP further hydrogenation can be neglected in the presence of sulfur-containing compounds. The hydrogenation of CHB to BCH is challenging (Figure 3F). Therefore, it is speculated that BCH is primarily obtained through the desulfurization of intermediate compounds produced by deep hydrogenation of DBT, rather than further hydrogenation of CHB. Additionally, no isomerization products are formed in BP hydrogenation even in the presence of H_2S. Thus, isomerization products may be derived from hydrogenated sulfur-containing intermediates, such as THDBT, HHDBT and DHDBT. This is different from the previous reports in which the isomerization products were obtained from the isomerization of CHB and/or BCH.[53,54]

Based on the performance of BP hydrogenation and analysis of the whole HDS reaction process over all catalysts, it is reliably demonstrated that the 1T phase is highly conducive to hydrogenation, while the S vacancy favors desulfurization. Indeed, a linear correlation is observed between the catalytic performance and the 1T phase content, as well as desulfurization and S vacancies (Figures 5A and 5B), which further verify that the aforementioned structure-function relationships that higher 1T content can enhance the hydrogenation, and the

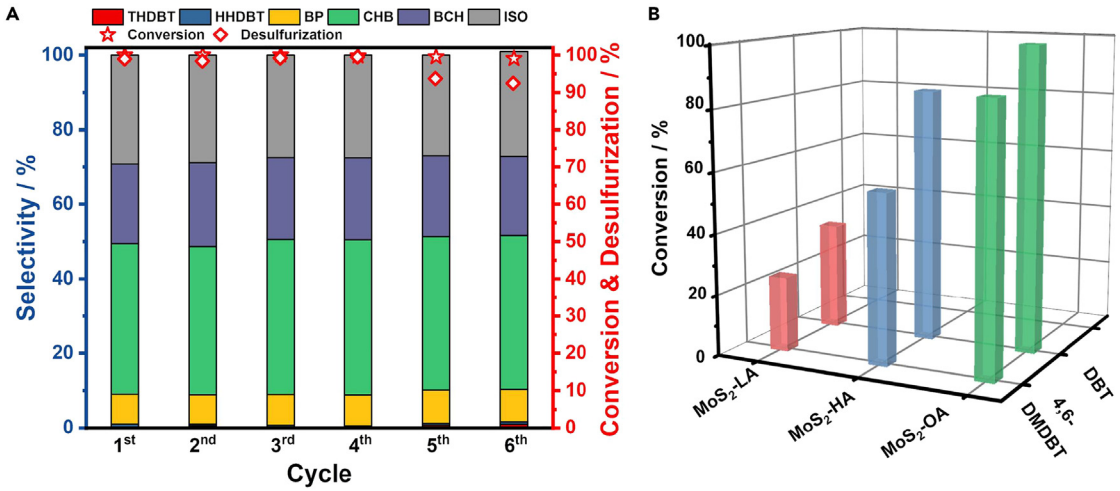

Figure 6. Catalytic stability test over MoS_2-OA and comparison of HDS activity on various catalysts

(A) The HDS performance of DBT on MoS_2-OA in 6 cycles.

(B) The HDS of DBT and 4,6-DMDBT on various catalysts.

desulfurization process is mainly driven by S vacancies over MoS_2 in HDS. This work takes a big step forward in determining the catalytic effect of 1T phase and S vacancies, and thereby provides a more comprehensive understanding of HDS on MoS_2 catalysts.[24,26]

Possible isomerization reaction mechanisms

It's noteworthy that all catalysts obtained isomerization products. Regarding the requirement of acid sites for isomerization, we first studied the IR spectra of adsorbed pyridine to quantify the concentration of Brønsted acid (BAS).[55–57] MoS_2-OA has a higher concentration of -SH than MoS_2-HA because its peak intensity is significantly greater than that of MoS_2-HA. For MoS_2-LA, the results were not given because its signal is too weak to detect (Figure S6). Thus, the ^{1}H solid-state nuclear magnetic resonance (^{1}H NMR) spectra provided robust evidence to support the above Py-IR results of the surface sulfhydryl (-SH) groups. ^{1}H NMR spectra of all used MoS_2 samples in Figure 5C show two broad signals located at 7.0 and 0.5 ppm, which might be assigned to isolated -SH groups and -SH species that interacted with S vacancies,[58] respectively. The ^{1}H signal of all MoS_2 catalysts is dominated by chemical shift 7.0 ppm. MoS_2-OA exhibited a higher abundance of -SH groups than other catalysts. Based on the EPR results, as the content of S vacancies increases, ^{1}H NMR peaks tend to shift toward high field.[59]

Our results on the HDS experiments of DBT revealed that the isomerization selectivity from the lowest to the highest is as follows: MoS_2-LA< MoS_2-HA< MoS_2-OA. It is noteworthy that this trend appeared to be relatively proportional to the concentration of -SH groups. However, the -SH group's acidity is inadequate to catalyze the isomerization of CHB, BCH and BP hydrogenation intermediates. Therefore, we speculated that the isomerization originated from sulfur-containing carbonium ion intermediates which may be triggered by the proton-supplying capacity of the Brønsted acid of -SH itself. Meanwhile, the 1T phase MoS_2 favorable for hydrogenated-DBT generation. As a result, MoS_2-OA with the highest 1T phase and -SH content possesses the highest isomerization performance among all catalysts. MoS_2-LA has the lowest isomerization selectivity, followed by MoS_2-HA.

Accordingly, the possible HHDBT isomerization mechanism is proposed in Figure 5D. Once the addition of the first H by -SH group for HHDBT, the cleavage of the cycloalkyl C-S bonds occurred, while the sulfur-containing carbonium ion intermediates formed. The latter may lead to the rearrangement of the carbonium ion intermediates, resulting in the formation of a new carbocation and an isomerization reaction. Then the cleavage of aryl C-S occurs followed by hydrogenation accompanied by the production of CMPB. The reaction mechanism of DHDBT is analogous to HHDBT.

Therefore, the differences in isomerization performance over MoS_2 catalysts may be explained by the both hydrogenation ability originates from the content of 1T phase and weak acidic from the -SH.

Catalyst superiority

MoS_2-OA catalyst shows the best performance for DBT HDS among the reported catalysts (Table S1). Furthermore, the stability of MoS_2-OA was evaluated as another important indicator for practical application since it had already exhibited outstanding activity as mentioned above.[60] MoS_2-OA was reused in the HDS of DBT for six cycles continuously, and the results are summarized in Figure 6A, which indicates the good stability of MoS_2-OA during DBT HDS. In addition, the MoS_2-OA catalyst could still show outstanding HDS efficiency in treating the highly refractory organosulfur compound 4,6-DMDBT (Figure 6B). Thus, the excellent HDS activity and stability facilely achieved over our catalyst guarantee a feasible prospect in the industrial application.

Conclusions

In summary, the ammonium/amine-intercalated 1T-2H MoS_2 has been successfully employed in the HDS process for the first time. A high DBT conversion of 100% and a high ultra-deep sulfur removal of 98.9% can be achieved over organic amine-intercalated MoS_2-OA during the HDS, and MoS_2-OA also exhibited a good stability with over 90% sulfur removal even after six consecutive catalytic runs. Even in processing the highly refractory organosulfur compound 4,6-DMDBT, MoS_2-OA exhibited excellent HDS performance. Combined with the HDS performance and the characterization analyses, the unequivocal structure-activity relationships established for DBT HDS pinpoints the role of the 1T phase as hydrogenation sites and S vacancies for desulfurization, and -SH groups as the acidic sites. The 'intercalation-deintercalation' processes of interlayered MoS_2 is critical to the *in situ* generation of active sites. Compared with inorganic ammonium, the intercalation of organic amine in MoS_2 was able to generate higher amounts of 1T phase and S vacancies, and reconstruction induced by the deintercalation of interlayer species further enhanced S vacancies formation during HDS. The hydrogenation activity by 1T phase and Brønsted acidic by -SH groups would promote the isomerization hydrogenated-DBT.

This study not only enables a more rigorous comparison of intrinsic activities among MoS_2 which were derived from the *in situ* reconstruction of expanded MoS_2 with various interlayer spacings but also bridges the gap between interlayer chemistry and efficient HDS performance. It is anticipated to inspire the rational design of cost-efficient catalysts via further regulating the 'intercalation-deintercalation' process.

Limitations of the study

Our work demonstrates the highly efficient HDS driven by an *in-situ* reconstruction of expanded MoS_2 catalysts, which is originated from the high amount of 1T phase and S vacancies via the 'intercalation-deintercalation' processes. However, the mechanism of *in-situ* reconstruction of different intercalated MoS_2 still needs to be explored, which will also be the future research.

STAR★METHODS

Detailed methods are provided in the online version of this paper and include the following:

- KEY RESOURCES TABLE
- RESOURCE AVAILABILITY
  - Lead contact
  - Materials availability
  - Data and code availability
- EXPERIMENTAL MODEL AND STUDY PARTICIPANT DETAILS
- METHOD DETAILS
  - Catalysts synthesis
  - Catalysts characterization
  - HDS activity measurement
- QUANTIFICATION AND STATISTICAL ANALYSIS
- ADDITIONAL RESOURCES

SUPPLEMENTAL INFORMATION

Supplemental information can be found online at https://doi.org/10.1016/j.isci.2024.109824.

ACKNOWLEDGMENTS

This work was financially supported by the National Key R&D Program of China (2023YFA1507602 and 2018YFA0209402), Natural Science Foundation of China (22088101, 22175077, 22378030).

AUTHOR CONTRIBUTIONS

Y.T. conceived the idea for the project and directed the research. T.Y., Y.J., K.H., and W.Z. conducted materials synthesis, performed structural characterizations and catalytic test. T.Y., Y.J., K.H., Z.G., Q.G., and Y.T. analyzed the catalytic results. T.Y., Q.G., and Y.T. drafted the manuscript. All authors discussed and commented on the manuscript.

DECLARATION OF INTERESTS

The authors declare no competing financial interest.

Received: January 18, 2024
Revised: March 11, 2024
Accepted: April 24, 2024
Published: April 26, 2024

REFERENCES

1. Huang, T., Xu, J., and Fan, Y. (2018). Effects of concentration and microstructure of active phases on the selective hydrodesulfurization performance of sulfided CoMo/Al_2O_3 catalysts. Appl. Catal. B Environ. *220*, 42–56.
2. Martínez-Palou, R., and Luque, R. (2014). Applications of ionic liquids in the removal of contaminants from refinery feedstocks: an industrial perspective. Energy Environ. Sci. *7*, 2414–2447.
3. Zhang, C., Bao, W., Ma, S., Wang, C., Liu, Y., Liu, C., Sun, D., and Lu, Y. (2023). A novel ligand protection strategy based on lacunary polyoxometalate to precisely construct CoMoS active sites for hydrodesulfurization. Chem. Eng. J. *473*, 145459.
4. Shafiq, I., Shafique, S., Akhter, P., Yang, W., and Hussain, M. (2022). Recent developments in alumina supported hydrodesulfurization catalysts for the production of sulfur-free refinery products: A technical review. Catal. Rev. Sci. Eng. *64*, 1–86.
5. Weng, X., Cao, L., Zhang, G., Chen, F., Zhao, L., Zhang, Y., Gao, J., and Xu, C. (2020). Ultradeep hydrodesulfurization of diesel: Mechanisms, catalyst design strategies, and challenges. Ind. Eng. Chem. Res. *59*, 21261–21274.
6. Tanimu, A., and Alhooshani, K. (2019). Advanced hydrodesulfurization catalysts: A review of design and synthesis. Energy Fuels *33*, 2810–2838.
7. Aleksandrov, P.V., Reshetnikov, S.I., Bukhtiyarova, G.A., and Noskov, A. (2022). Deep hydrodesulfurization of gas oils with high sulfur content: Experiment and kinetic modeling. Chem. Eng. J. *446*, 137059.
8. Liu, J., Zhu, J., Zhu, J., Xu, J., Liu, H., Hua, M., Cheng, H., Li, H., Liu, J., Zhu, W., and Ji, H. (2023). One-pot three-dimensional printing of a hierarchical NiMo/Al_2O_3 monolithic catalyst for 4,6-dimethyldibenzothiophene hydrodesulfurization. ACS Appl. Mater. Interfaces *15*, 33593–33604.
9. Wang, L., Bai, Z., Zhang, X., and Li, G. (2022). Co-Doped MoS_2 nanosheets vertically grown on Ti_3C_2 MXenes for efficient hydrodesulfurization in high-temperature environments. ACS Appl. Nano Mater. *5*, 9666–9677.
10. Zhao, Y., Zheng, X., Gao, P., and Li, H. (2023). Recent advances in defect-engineered molybdenum sulfides for catalytic applications. Mater. Horiz. *10*, 3948–3999.
11. Walton, A.S., Lauritsen, J.V., Topsøe, H., and Besenbacher, F. (2013). MoS_2 nanoparticle morphologies in hydrodesulfurization catalysis studied by scanning tunneling microscopy. J. Catal. *308*, 306–318.
12. Venkateshwaran, S., Devi, P., Murugan, P., and Senthil Kumar, S.M. (2024). Simple immersion in polar solvents induces targeted 1T phase conversion of MoS_2 for HER: A greener approach. ACS Appl. Energy Mater. *7*, 1037–1050.
13. Fang, Y., Pan, J., He, J., Luo, R., Wang, D., Che, X., Bu, K., Zhao, W., Liu, P., Mu, G., et al. (2018). Structure re-determination and superconductivity observation of bulk 1T MoS_2. Angew. Chem. Int. Ed. *57*, 1232–1235.
14. Bruix, A., Lauritsen, J.V., and Hammer, B. (2021). Size-dependent phase stability in transition metal dichalcogenide nanoparticles controlled by metal substrates. Nanoscale *13*, 10167–10180.
15. Zhao, X., Ning, S., Fu, W., Pennycook, S.J., and Loh, K.P. (2018). Differentiating polymorphs in molybdenum disulfide via electron microscopy. Adv. Mater. *30*, 1802397.
16. Zheng, P., Duan, A., Chi, K., Zhao, L., Zhang, C., Xu, C., Zhao, Z., Song, W., Wang, X., and Fan, J. (2017). Influence of sulfur vacancy on thiophene hydrodesulfurization mechanism at different MoS_2 edges: A DFT study. Chem. Eng. Sci. *164*, 292–306.
17. Zhang, T., Bai, Z., Wang, L., Zhang, X., and Li, G. (2023). Modulating crystallization of MoS_2 nanostructures by dimethyl sulfoxide for enhanced hydrodesulfurization. ACS Appl. Nano Mater. *6*, 21752–21762.
18. Mom, R.V., Louwen, J.N., Frenken, J.W.M., and Groot, I.M.N. (2019). In situ observations of an active MoS_2 model hydrodesulfurization catalyst. Nat. Commun. *10*, 2546.
19. Aireddy, D.R., and Ding, K. (2022). Heterolytic dissociation of H_2 in heterogeneous catalysis. ACS Catal. *12*, 4707–4723.
20. Jing, Y., and Wang, Y. (2023). Heterolytic dissociation of H_2 and bond activation: Spotting new opportunities from a unified view. Chem Catal. *3*, 100515.
21. Zhao, Y., Chang, K., Gu, Q., Yang, B., Xu, J., Zhang, Y., Pan, C., Wang, Z., Lou, Y., and Zhu, Y. (2022). Noble metal-free 2D 1T-MoS_2 edge sites boosting selective hydrogenation of maleic anhydride. ACS Catal. *12*, 8986–8994.
22. Shang, H., Wang, T., and Zhang, W. (2019). Sulfur vacancy formation at different MoS_2 edges during hydrodesulfurization process: A DFT study. Chem. Eng. Sci. *195*, 208–217.
23. Sun, K., Guo, H., Jiao, F., Chai, Y., Li, Y., Liu, B., Mintova, S., and Liu, C. (2021). Design of an intercalated nano-MoS_2 hydrophobic catalyst with high rim sites to improve the hydrogenation selectivity in hydrodesulfurization reaction. Appl. Catal. B Environ. *286*, 119907.
24. He, S.S., Huang, T.T., Chen, C., and Fan, Y. (2023). Tuning active sites in MoS_2-based catalysts via H_2O_2 etching to enhance hydrodesulfurization performance. Petrol. Sci. *20*, 3875–3886.
25. Chen, J., Wu, S., Zhang, X., and Liu, Y. (2023). Few-layered defect-rich MoS_2 nanosheets with Ni doping as catalysts for efficient hydrodesulfurization reaction. ACS Appl. Nano Mater. *6*, 18812–18822.
26. Cao, H., Bai, Z., Li, Y., Xiao, Z., Zhang, X., and Li, G. (2020). Solvothermal synthesis of defect-rich mixed 1T-2H MoS_2 nanoflowers for enhanced hydrodesulfurization. ACS Sustain. Chem. Eng. *8*, 7343–7352.
27. Bai, Z., Wang, L., Cao, H., Zhang, X., and Li, G. (2022). Symbiosis of 1T and 2H phases in the basal plane of defective MoS_2 nanoflowers for efficient hydrodesulfurization. Fuel *322*, 124252.
28. Wei, J., Huang, H., Luo, Q., Liu, N., Wang, X., Wang, X., Zhong, M., and Huang, X. (2022). Synthesis of few layer amorphous 1T/2H MoS_2 by a one-step ethanol/water solvothermal method and its hydrodesulfurization performance. Catal. Lett. *152*, 263–275.
29. Tan, J., Zhang, W., Shu, Y., Lu, H., Tang, Y., and Gao, Q. (2021). Interlayer engineering of molybdenum disulfide toward efficient electrocatalytic hydrogenation. Sci. Bull. *66*, 1003–1012.
30. Tan, J., Shao, J., Shi, Y., Zhang, W., and Gao, Q. (2022). Selective electrocatalytic hydrogenation of nitroarenes on interlayer-expanded MoS_2. ACS Sustain. Chem. Eng. *10*, 13525–13533.
31. Dong, H., Xu, Y., Zhang, C., Wu, Y., Zhou, M., Liu, L., Dong, Y., Fu, Q., Wu, M., and Lei, Y. (2018). MoS_2 nanosheets with expanded interlayer spacing for enhanced sodium storage. Inorg. Chem. Front. *5*, 3099–3105.
32. Xie, J., Zhang, J., Li, S., Grote, F., Zhang, X., Zhang, H., Wang, R., Lei, Y., Pan, B., and Xie, Y. (2013). Controllable disorder engineering in oxygen-incorporated MoS_2 ultrathin nanosheets for efficient hydrogen evolution. J. Am. Chem. Soc. *135*, 17881–17888.
33. Lei, Z., Zhan, J., Tang, L., Zhang, Y., and Wang, Y. (2018). Recent development of metallic (1T) phase of molybdenum disulfide for energy conversion and storage. Adv. Energy Mater. *8*, 1703482.
34. Wang, D., Xiao, Y., Luo, X., Wu, Z., Wang, Y.J., and Fang, B. (2017). Swollen ammoniated MoS_2 with 1T/2H hybrid phases for high-rate electrochemical energy storage. ACS Sustain. Chem. Eng. *5*, 2509–2515.
35. Wu, Z., Tang, C., Zhou, P., Liu, Z., Xu, Y., Wang, D., and Fang, B. (2015). Enhanced hydrogen evolution catalysis from osmotically swollen ammoniated MoS_2. J. Mater. Chem. A *3*, 13050–13056.
36. Jayabal, S., Wu, J., Chen, J., Geng, D., and Meng, X. (2018). Metallic 1T-MoS_2 nanosheets and their composite materials: Preparation, properties and emerging applications. Mater. Today Energy *10*, 264–279.
37. Zhao, D., Xu, S., Wang, H., Shen, Y., and Xu, Q. (2023). Exfoliation of MoS_2 by zero-valent transition metal intercalation. Chem. Commun. *59*, 8135–8138.
38. Jin, H., Yu, Y., Shen, Q., Li, P., Yu, J., Chen, W., Wang, X., Kang, Z., Zhu, L., Zhao, R., et al. (2021). Direct synthesis of 1T-phase MoS_2 nanosheets with abundant sulfur-vacancies through $(CH_3)_4N^+$ cation-intercalation for the hydrogen evolution reaction. J. Mater. Chem. A *9*, 13996–14003.
39. Geng, X., Sun, W., Wu, W., Chen, B., Al-Hilo, A., Benamara, M., Zhu, H., Watanabe, F., Cui, J., and Chen, T.P. (2016). Pure and stable metallic phase molybdenum disulfide nanosheets for hydrogen evolution reaction. Nat. Commun. *7*, 10672.
40. Ma, Y., Leng, D., Zhang, X., Fu, J., Pi, C., Zheng, Y., Gao, B., Li, X., Li, N., Chu, P.K., et al. (2022). Enhanced activities in alkaline hydrogen and oxygen evolution reactions on MoS_2 electrocatalysts by in-plane sulfur defects coupled with transition metal doping. Small *18*, 2203173.
41. Wang, X., Zhang, Y., Si, H., Zhang, Q., Wu, J., Gao, L., Wei, X., Sun, Y., Liao, Q., Zhang, Z., et al. (2020). Single-atom vacancy defect to trigger high-efficiency hydrogen evolution of MoS_2. J. Am. Chem. Soc. *142*, 4298–4308.
42. Li, P., Chen, Y., Zhang, C., Huang, B., Liu, X., Liu, T., Jiang, Z., and Li, C. (2017). Highly selective hydrodesulfurization of gasoline on unsupported Co-Mo sulfide catalysts: Effect of MoS_2 morphology. Appl. Catal. Gen. *533*, 99–108.
43. Zhu, J., Wang, Z., Yu, H., Li, N., Zhang, J., Meng, J., Liao, M., Zhao, J., Lu, X., Du, L., et al. (2017). Argon plasma induced phase transition in monolayer MoS_2. J. Am. Chem. Soc. *139*, 10216–10219.
44. Li, L., Qin, Z., Ries, L., Hong, S., Michel, T., Yang, J., Salameh, C., Bechelany, M., Miele, P., Kaplan, D., et al. (2019). Role of sulfur

vacancies and undercoordinated Mo regions in MoS_2 nanosheets toward the evolution of hydrogen. ACS Nano *13*, 6824–6834.

45. Bello, S.S., Wang, C., Zhang, M., Gao, H., Han, Z., Shi, L., Su, F., and Xu, G. (2021). A review on the reaction mechanism of hydrodesulfurization and hydrodenitrogenation in heavy oil upgrading. Energy Fuels *35*, 10998–11016.
46. Yang, L., Li, X., Wang, A., Prins, R., Chen, Y., and Duan, X. (2015). Hydrodesulfurization of dibenzothiophene, 4,6-dimethyldibenzothiophene, and their hydrogenated intermediates over bulk tungsten phosphide. J. Catal. *330*, 330–343.
47. Wagenhofer, M.F., Shi, H., Gutiérrez, O.Y., Jentys, A., and Lercher, J.A. (2020). Enhancing hydrogenation activity of Ni-Mo sulfide hydrodesulfurization catalysts. Sci. Adv. *6*, eaax5331.
48. Niu, H., Wang, X.B., Luo, J., Liu, J., Li, C., Li, W.Y., and Liang, C. (2023). C-S cleavage of dibenzothiophenes with or without steric hindrance by the interface between PtS_x and ZnO. Chem. Eng. J. *470*, 144115.
49. Bai, J., Li, X., Wang, A., Prins, R., and Wang, Y. (2012). Hydrodesulfurization of dibenzothiophene and its hydrogenated intermediates over bulk MoP. J. Catal. *287*, 161–169.
50. Zheng, P., Xiao, C., Cao, Z., Shi, Y., Wang, G., Duan, A., and Xu, C. (2021). DFT insights into the hydrodesulfurization mechanisms of different sulfur-containing compounds over CoMoS active phase: Effect of the brim and CUS sites. Chem. Eng. Sci. *231*, 116311.
51. Hu, Y., Kuang, S., Zhou, X., Li, X., Zhang, S., Prins, R., Zhang, C., Shang, S., and Sheng, Q. (2023). Insights into Correlations among the hydrodesulfurization, hydrodenitrogenation, and hydrogen evolution reactions over molybdenum phosphide catalysts modified by cerium oxide. ACS Catal. *13*, 13786–13803.
52. Rajendran, A., Cui, T.Y., Fan, H.X., Wang, M.Y., and Li, W.Y. (2022). High-performance NiMoS hydrodesulfurization catalysts by one-pot hydrothermal synthesis using $Ni(acac)_2$ for sulfur-free liquid fuels. Fuel Process. Technol. *227*, 107101.
53. Sharifvaghefi, S., Yang, B., and Zheng, Y. (2018). New insights on the role of H_2S and sulfur vacancies on dibenzothiophene hydrodesulfurization over MoS_2 edges. Appl. Catal. Gen. *566*, 164–173.
54. Liu, X., Liu, J., Li, L., Zhang, X., Sun, H., Guo, R., Ren, S., Guo, Q., Wen, X.D., and Shen, B. (2020). Preparation of electron-rich Fe-based catalyst via electronic structure regulation and its promotion to hydrodesulfurization of dibenzothiophene. Appl. Catal. B Environ. *269*, 118779.
55. Li, X., Zhou, X., Wang, L., Lv, J., Liu, S., Prins, R., Wang, A., and Sheng, Q. (2021). Mechanistic studies and kinetics of the desulfurization of 2-phenylcyclohexanethiol over sulfided Mo, Ni-Mo, and Co-Mo on γ-Al_2O_3. J. Catal. *403*, 43–55.
56. Luo, W., Shi, H., Schachtl, E., Gutiérrez, O.Y., and Lercher, J.A. (2018). Active sites on nickel-promoted transition-metal sulfides that catalyze hydrogenation of aromatic compounds. Angew. Chem. Int. Ed. *57*, 14555–14559.
57. Topsøe, H., Clausen, B.S., and Massoth, F.E. (1996). Hydrotreating Catalysis (Springer).
58. Ai, K., Ruan, C., Shen, M., and Lu, L. (2016). MoS_2 nanosheets with widened interlayer spacing for high-efficiency removal of mercury in aquatic systems. Adv. Funct. Mater. *26*, 5542–5549.
59. Yao, Q., Zhang, L., Huang, D., Ding, H., Feng, W., Zhang, J., Ren, Y., Chen, X., Yue, B., and He, H. (2023). MAS NMR studies on the formation and structure of oxygen vacancy on the CeO_2 {110} surface under a reducing atmosphere. J. Phys. Chem. C *127*, 13021–13033.
60. Kang, X., Wang, D., Liu, J., Tian, C., Xu, H., Xu, J., and Fu, H. (2022). Ni-promoted MoS_2 in hollow zeolite nanoreactors: enhanced catalytic activity and stability for deep hydrodesulfurization. J. Mater. Chem. A *10*, 7263–7270.
61. Jia, Y., Hu, A., Hu, D., Li, M., Li, H., Yang, Q., Liu, Z., Shao, Z., Zeng, S., Zhao, X., and Wang, Y. (2024). Design of active phase structure with high activity and stability in residue hydrotreating reactions. Fuel *360*, 130288.

STAR★METHODS

KEY RESOURCES TABLE

REAGENT or RESOURCE	SOURCE	IDENTIFIER
Chemicals, peptides, and recombinant proteins		
Ammonium heptamolybdate	Sinopharm Chemical Reagent Co., Ltd	CAS 12027-67-7
Thiourea	Sinopharm Chemical Reagent Co., Ltd	CAS 62-56-6
N,N-dimethylformamide	Sinopharm Chemical Reagent Co., Ltd	CAS 68-12-2
Cyclohexylbenzene	Tokyo Chemical Industry Co., Ltd	CAS 827-52-1
Bicyclohexane	Tokyo Chemical Industry Co., Ltd	CAS 92-51-3
Dibenzothiophene	Aladdin Ltd (Shanghai, China)	CAS 132-65-0
Biphenyl	Aladdin Ltd (Shanghai, China)	CAS 92-52-4
Decalin	Sigma-Aldrich	CAS 91-17-8
Software and algorithms		
OriginPro Learning Edition	OriginLab	https://www.originlab.com/

RESOURCE AVAILABILITY

Lead contact

Further information and requests for resources and materials should be directed to and will be fulfilled by the lead contact, Yi Tang (yitang@fudan.edu.cn).

Materials availability

This study did not generate new unique reagents. All catalysts generated in this work are available from the lead contact upon request.

Data and code availability

- The datasets generated in this study are available from the lead contact upon request.
- This work does not report original code.
- Any additional information required to reanalyze the data reported in this paper can be obtained from the lead contact upon request.

EXPERIMENTAL MODEL AND STUDY PARTICIPANT DETAILS

This study does not use experimental models.

METHOD DETAILS

Catalysts synthesis

All catalysts used in this study were prepared through a facile one-step hydrothermal reaction. In a typical synthesis, 0.282 g of ammonium heptamolybdate and 1.464 g of thiourea were dissolved in a mixed solvent containing 8 mL of deionized water and 4 mL of N,N-dimethylformamide. The mixture was ultrasonic treatment for 15 min and magnetically stirred for 30 min to form a transparent solution, the solution was transferred to a 25 mL Teflon-lined autoclave and heated to 180°C for 4 h. The autoclave was then cool to room temperature naturally, and the product was collected by centrifugation. Finally, the obtained product was rinsed thoroughly with deionized water and ethanol for several times and then dried at 60°C under vacuum. The resulting product was named MoS_2-OA.

Similarly, the MoS_2-HA was prepared by following same procedures described above except for only using deionized water as the solvent but in absence of N,N-dimethylformamide. For comparison, MoS_2-LA were synthesized from identical precursors through hydrothermal treatment at 180°C for a long time to eliminate NH_4^+ intercalation using deionized water as solvent.

Catalysts characterization

Powder X-ray diffraction (XRD) patterns were obtained on a Bruker D2 diffractometer (Germany), using copper Kα radiation (λ = 0.154056 nm) at 30 kV and 10 mA in the 2θ scanning range of 5-80° at a scanning rate of 5° min^{-1}. The morphology and energy dispersive spectroscopy (EDS) of catalysts were investigated by using a high-resolution transmission electron microscopy (HRTEM, FEI Tecnai G2 F20 S-Twin). Element

compositions were determined by inductively coupled Plasma Optical Emission Spectrometer (ICP-OES) on AGILENT 730 (USA). Raman spectrum is collected on the laser confocal Raman microspectrometer (XploRA, Horiba Jobin Yvon, Ltd.) with an excitation wavelength of 532 nm. X-ray photoelectron spectroscopy (XPS) is collected by scanning X-ray microprobe (Thermo Scientific, ESCALAB 250Xi) using Al Kα radiation and the C 1s peak at 284.8 eV as the internal standard. Electron paramagnetic resonance (EPR) spectra were obtained using a JEOL JES FA200 spectrometer. Temperature programmed reduction using hydrogen (H_2-TPR) were conducted on Micromeritics Autochem 2920 chemisorption instrument. For H_2-TPR experiment, the samples were pretreated at 130°C for 1h in Ar flow to remove impurities and adsorbed water from sample surface. After cooling to room temperature, H_2-TPR analyses were carried out in a 5 vol% H_2/Ar flow of 20 mL min^{-1} from room temperature to 800°C. ^{1}H MAS NMR experiments were recorded on a Bruker AVANCE III 400 WB spectroscope at 400 MHz. Adamantane was used as the external standard both for the chemical shift and the quantification of the ^{1}H molar number corresponded to related peaks.

HDS activity measurement

The catalytic performance in HDS was carried out in a 100 mL batch reactor (Shanghai LABE Instrument Co., Ltd) using DBT as a model sulfur compound with a concentration of 330 ppm of sulfur content corresponding to decalin solvent. Typically, 50 mg of catalyst and 20 mL model fuel transferred to the batch reactor. Prior to the activity test, the reactor was purged with H_2 for five times, and then the initial H_2 pressure at room temperature was controlled at 3.5 MPa with a stirring speed of 500 rpm. Normally, the total pressure in the sealed reactor gradually increased to 6.0 MPa along with the reaction temperature reached 320°C. After reaction, the liquid-phase products were collected and analyzed by gas chromatograph (Shimadzu, GC 2010 plus) equipped with HP-5 column (30 m × 0.32 mm × 0.25 μm) and flame ionization detector. To further identify each of the compounds in the liquid products, GC-MS (Shimadzu, GCMS-QP2010 SE) with a HP-5 capillary column (30 m × 0.25 mm × 0.25 μm) was used to analyze the collected products.

There are seven main products after the HDS of DBT, which are tetrahydro-dibenzothiophene (THDBT), hexahydro-dibenzothiophene (HHDBT), biphenyl (BP), cyclohexylbenzene (CHB), bicyclohexane (BCH), (cyclopentylmethyl)benzene (CPMB) and (cyclopentylmethyl)cyclohexane (CPMC). The conversion (X) of DBT and the selectivity (S_i) of products were defined as follows equations:[51]

$$X\,(\%) = \left(1 - \frac{n_t}{n_0}\right) \times 100\%$$

$$S_i\,(\%) = \frac{n_i}{n_0 - n_t} \times 100\%$$

where n_0 and n_t refer to the molar concentrations of DBT in the feed and products, respectively, and n_i refer to the HDS products of DBT in the reaction.

It is well known that HDS of DBT occurs two pathways: (i) direct desulfurization (DDS) and (ii) hydrogenation (HYD).[47,48] It has been reported in many previous literatures that THDBT, HHDBT, CHB, BCH, CPMB and CPMC are main products for the HYD pathway, while the BP is the product of DDS pathway. The selectivity of the HYD reaction and DDS reaction pathway ($S_{HYD/DDS}$) can be calculated by the equations as follows:[52]

$$Selectivity\ of\ DDS\ (\%) = \left(\frac{n_{BP}}{n_{THDBT}+n_{HHDBT}+n_{BP}+n_{CHB}+n_{BCH}+n_{CPMB}+n_{CPMC}}\right) \times 100\%$$

$$Selectivity\ of\ HYD\ (\%) = \left(\frac{n_{THDBT}+n_{HHDBT}+n_{CHB}+n_{BCH}+n_{CPMB}+n_{CPMC}}{n_{THDBT}+n_{HHDBT}+n_{BP}+n_{CHB}+n_{BCH}+n_{CPMB}+n_{CPMC}}\right) \times 100\%$$

$$S_{HYD/DDS} = \frac{S_{HYD}}{S_{DDS}}$$

Meanwhile, the total sulfur content was determined using sulfur-nitrogen analyzer (Jiangsu Guochuang Analytical Instrument Co., Ltd, GCTNS-3000). The standard curve of the integral area corresponding to the total sulfur content is established with the standard samples with different sulfur contents. The sulfur removal rate (S) of DBT was defined as follows:[61]

$$S\,(\%) = \frac{S_f - S_p}{S_f} \times 100\%$$

in the above equations, S_f and S_p represent the sulfur content in the feed and products, respectively.

For the catalytic reusability experiments, the cyclic reaction procedure to evaluate the stability of the MoS_2-OA was the same as that used for evaluating the fresh catalyst. The used catalyst was separated by centrifugation after the reaction, washed thoroughly with decalin used for the next run, and the same procedure was repeated before every successive catalytic run.

The pseudo first-order reaction model was adopted in the hydrodesulfurization reaction of DBT, and the reaction rate ($\mu mol \cdot g_{cat}^{-1} \cdot s^{-1}$) was calculated at low conversion based on the following formula:[47]

$$r_{HDS} = \frac{W_{DBT} \times X}{M_{DBT} \times t}$$

where W_{DBT} denotes the weight fraction of DBT in the reactant and M_{DBT} denotes the molecular mass of DBT.

QUANTIFICATION AND STATISTICAL ANALYSIS

This study does not include statistical analysis or quantification.

ADDITIONAL RESOURCES

This work does not include any additional resource.